IGPP Final Report

DIRECT AND INDIRECT FORCING OF OCEANIC INFRAGRAVITY WAVES BY THE ATMOSPHERE: Origins of the Continuous Earth Oscillations

D.O. ReVelle[1] and T. Tanimoto[2]

[1]Atmospheric, Climate and Environmental Dynamics Group
Earth and Environmental Sciences Division
P.O. Box 16763, MS D401
Los Alamos National Laboratory
Los Alamos New Mexico 87545

[2]Department of Geological Sciences, Webb Hall-Building 526
University of California at Santa Barbara
Santa Barbara, California 93106

October 2004

I. Introduction and Overview

Calculations have been performed at Los Alamos National Laboratory in the Earth and Environmental Science Division in direct support of IGPP grant:

Continuous Free Oscillations and its Application to Planetary Seismology

We have determined that the relevant continuous free oscillations of the Earth are driven by the world's oceans (Tanimoto and ReVelle, 2004). We now present arguments and specific calculations illustrating how the oceanic oscillations themselves are excited by the large scale atmosphere. The full details of these calculations are provided below.

II. Mathematical/Physical Modeling

A. Atmospheric Modeling

Atmospheric modeling was accomplished assuming a hydrostatic isothermal or non-isothermal fluid model that is in a horizontally stratified and steady-state equilibrium and which is not dependent upon range (One-dimensional model with perfect stratification). Isothermal conditions at all altitudes were specified by assuming a ground-level temperature value = 250 K (this is a suitable mean value for the height interval from the ground up to 120 km altitude with a corresponding mean adiabatic, thermodynamic sound speed over this height interval of ~316.97 m/s). Mean molecular weight values were calculated as a function of height with values allowed to systematically decrease above

~85 km because of photo-dissociation and photo-ionization produced by the ultraviolet part of the arriving electromagnetic solar spectrum.

The combination of these parameters of temperature, sound speed and mean molecular weight allowed both the pressure and density scale heights to be computed at all heights. From these scale height values the pressure and density values as a function of height were obtainable by vertical integrations over small altitude intervals (0.25 km was used throughout). In addition, from the vertical temperatures and associated vertical temperature gradients, we computed the resonant frequencies of the atmosphere for this part of the atmospheric wave spectrum for acoustic-gravity waves (AGW), i.e., the acoustic waveguide cut-off frequency and the corresponding Brunt-Vaisalla frequency. The mean sound speed profiles for summer and the predicted resonant AGW frequencies of the atmosphere (using either the isothermal or the non-isothermal approximations) are given below in Figures 1 and 3. The mean sound speed profiles for winter and the predicted resonant AGW frequencies of the atmosphere (using either the isothermal or the non-isothermal approximations) are given below in Figures 7 and 9.

The non-isothermal atmospheric temperature structure that was computed reproduces the general form of the latest U.S. Standard Atmosphere models that have been developed at middle latitudes for the summer and winter seasons. The computed horizontal winds for the models in summer and winter are also indicative of a quasi-geostrophic flow regime (Ro < ~ 0.50) at all heights which is fully justified on the basis of the computed Rossby number, Ro, of the flows for both seasons (see also below). Thus, these winds were calculated as if the Rossby number were exactly zero throughout, i.e., as if the atmosphere was in a state of hydrostatic and geostrophic equilibrium. The alternatives to this computation were to go to a truly global scale dynamical numerical weather prediction model which was well beyond the scope of the current very limited study. Typical summer and winter profiles of the calculated horizontal winds are plotted in Figures 2 and 8 respectively.

B. Direct Forcing (DF): Forcing by Surface Boundary Layer Winds

We had previously hoped to be able to calculate the direct pressure forcing of the ocean by the low-level mean atmospheric winds using my very detailed one-dimensional, time dependent code BLMARC.f. Unfortunately although the winds are predicted in great detail, additional knowledge is not available from the code to directly predict the corresponding pressure perturbations at the lower model boundary. the lowest-level winds directly (DF forcing) to examine oceanic forcing An estimation of the DF cannot be done without some independent information on air density (assuming also for example that an ideal gas is an adequate approximation near the earth’s surface which is an increasingly less accurate approximation as the atmospheric pressure increases) during the corresponding wind and temperature calculations.

It should be noted that although we have been unable to solve the DF problem in terms of surface pressure wave generation, the connection to the IF below are readily apparent. It is well-known for example that the near-surface boundary layer winds are directly a function of the prevailing synoptic scale geostrophic wind (Gill, 1982). It is however the vertical shear of the prevailing geostrophic winds and the inherent dynamic Kelvin-Helmholtz instability (possibly other types of

instability contribute to this process as well) that results in the presence of turbulent shear layers aloft that is driving the internal gravity waves that we have calculated below.

Anticipating our results below, we note that the magnitude of the pressure perturbations that we have predicted at the surface by internal gravity waves propagating downward from an unstable wind shear layer centered at the Polar tropospheric jet stream are comparable to a near-surface wind of ~0.5 to 3.5 m/s (using dynamic pressure arguments that show that the perturbation pressure is proportional to the product of air density and the square of the local perturbation wind speed). This range of near-surface wind speed values is certainly comparable to the observed surface boundary layer winds that regularly develop over the world's oceans under non-stormy weather conditions.

C. Indirect Forcing (IF): Forcing by Shear Instability Aloft

Dynamic meteorologists have long known that regions of wind shear aloft can be unstable and develop turbulence through such dynamical instability and subsequently radiate both acoustic (Stein, 1967; Musielak et. al., 1994) as well as internal gravity waves (Herron, Tolstoy and Kraft, 1969, Herron and Tolstoy, 1969, Tolstoy and Herron, 1969, McIntosh and ReVelle, 1984; Gavrilov, 1997, Grigor'ev, 1999, Nappo, 2002, Hines, 2002). The vast majority of investigations on this subject have been regarding the effects of this wave excitation/radiation process for corresponding upward propagation and its effects on either the lower thermosphere/ionosphere of the earth or on solar/stellar heating scenarios (Stein, 1967; Muslielak et. al., 1994; Gavrilov, 1997). This large degree of interest derives directly from simple inviscid fluid arguments regarding the conservation of the wave kinetic energy density and the expected degree of wave amplification for vertically upward propagation paths.

In this very limited IGPP study, we have examined a linear analytical, nondissipative (inviscid and non-heat conducting) prediction model (Tolstoy and Herron, 1969; Gavrilov, 1997) for the propagating internal gravity wave part of the AGW spectrum for downward propagation of wave energy from regions of dynamic wind shear instability aloft to the earth's surface. The air is assumed to be well above the dew point temperature so it can be treated as a dry ideal gas, i.e., with no phase changes of water vapor occurring such as condensation, etc. In this study, we have neglected internal gravity wave breaking phenomena (Lindzen, 1985), the formation of critical layers (where rapid energy transfer occurs when the wave phase speed matches the wind speed) as well as wave saturation effects (Weinstock, 1996), since these are far less likely to be important for these downward propagating waves into an increasingly more dense medium (for which wave behavior becomes progressively more linear, i.e., in the small amplitude limit). In addition, our model results are in effect already calibrated since the predicted model levels have already been shown to be comparable to the observed wave fields measured during the passage of the tropospheric Polar jet stream to the vicinity of ground-based microbarograph arrays. Herron and Tolstoy (1969) have previously reported that these ground level observations were observed to continue for weeks at a time.

We have examined the results of this downward propagation for mean profiles for both the summer and winter seasons for middle altitudes for the earth's atmosphere. The motivation for this prediction was to determine if the atmosphere could excite the ocean by radiating an internal gravity wave field of the proper amplitude and wave period in order to excite the continuous earth oscillation modes. Thus, wave periods of propagating AGW from the local Brunt-Vaisalla period to ~3 hours in period were examined.

Wave Source Description:

The model of Tolstoy and Herron (1969) is well rooted in both theory as well as in observations and has previously been shown to provide the proper level of ground-level amplitude to explain the microbarograph observations of Herron and Tolstoy (1969) from the core of the Polar Tropospheric Jet Stream aloft (heights from ~8-12 km in middle latitudes). Briefly, the model assumes a region of dynamic instability aloft where internal gravity waves are radiated within a zone centered at the wind shear concentration axis. Thus, the atmosphere in this approximation provides a zone of pressure waves dragged along by the jet stream axis to propagate downward to distances as much as +/- ~200 km away from the jet stream axis, but exists at all longitudes around the earth for which the jet stream is dynamically unstable (synoptic scale meteorological regime). Furthermore, this dynamical source region exists in both hemispheres simultaneously, albeit with a large range of possible amplitudes and wave periods as a function of season (see below for further details). This source sets up a standing wave pattern in the vertical plane of propagating pressure waves that are dragged along by the jet stream at its travel speed aloft, so that the source is in continuous motion from West to East in both hemispheres at all times. The source height in this conceptual model is an integral number of vertical wavelengths above the ground. We have calculated the vertical wavenumber of such waves using linear AGW perturbation theory (Mihalas and Mihalas, 1984; Holton, 1992) as shown below.

It is well known that the pattern of Rossby wave activity in both hemispheres waxes and wanes in time and changes from a region of low index cycle to one of a large index cycle in a time periods of ~20-60 days, but whose oscillation period is fundamentally unpredictable (Petterson, 1969). This oscillation cycle exhibits periods of large Rossby wave amplitude and high winds and numerous middle latitude storms followed by period of nearly symmetric wave flow about the poles with correspondingly small Rossby wave amplitude and light winds and comparatively few storms (Holton, 1992). We are currently examining the basic set of global seismic data to determine if such periodicity is evident in the observations and their changes with time.

Instead of restricting ourselves to the Polar Tropospheric Jet Stream as a source of these waves, in this IGPP study, we have calculated this wind shear continuously at all heights and allowed the resulting dynamic instability to directly determine the zones of instability as a function of height and season and to calculate the corresponding amplitudes and wave periods at ground-level for each of these sources.

We have used the following set of calculation equations in this study:

Atmospheric parameters: Vertical Scales and Resonant Frequencies, etc.:

$H_p(z) = RT(z)/g$ = Pressure scale height ($\equiv -p(z)/\partial p(z)/\partial z$)

$H_\rho(z) = H_p(z)/(1+\{R\cdot\partial T/\partial z/g\})$= Density scale height ($\equiv -\rho\ /\partial\rho/\partial z$)

$R = R^*/M$= Universal gas constant/Mean molecular weight

$\rho(z) = \rho_o\cdot\exp[-\int dz/H_\rho(z)]$= Air density as a function of geopotential altitude

$p(z) = p_o\cdot\exp[-\int dz/H_p(z)]$= Atmospheric pressure as a function of geopotential altitude

$c_s(z) = \{\gamma RT(z)\}^{1/2}$

" = Adiabatic, thermodynamic sound speed as a function of height

g = Acceleration due to gravity (=9.8066 m/s^2)

γ = Specific heat ratio for an assumed ideal, diatomic gas ($\cong$ 1.40)

$\omega_{BVI}(z) = \{(\gamma-1)g^2/c_s^2\}^{1/2}$ = Angular <u>isothermal</u> Brunt-Vaisalla (resonant) frequency

$\omega_{ACI}(z) = \gamma g/(2c_s)$ = Angular <u>isothermal</u> acoustic waveguide cut-off frequency

$\omega_{BV}(z) =\{\omega_{BVI}^2 + (g/T(z))\cdot\partial T(z)/\partial z\}^{1/2}$ =

* " = Angular non-isothermal Brunt-Vaisalla (resonant) frequency

$\omega_{AC}(z) = \{\omega_{ACI}^2 + (\gamma/2)(g/T(z)\cdot\partial T(z)/\partial z\}^{1/2}$ =

" = Angular non-isothermal acoustic waveguide cut-off frequency

$\tau_{BVI}(z) = \{2\cdot\pi)/\omega_{BVI}(z)\}$ = Isothermal Brunt-Vaisalla resonant wave period

$\tau_{ACI}(z) = \{2\cdot\pi/\omega_{ACI}(z)\}$ = Isothermal acoustic cut-off resonant wave period

$\tau_{BV}(z) = \{2\cdot\pi\}/\omega_{BV}(z)\}$ = Nonisothermal Brunt-Vaisalla resonant wave period

$\tau_{AC}(z) = \{2\cdot\pi\}/\omega_{AC}(z)\}$ = Nonisothermal acoustic cut-off resonant wave period

$\partial W(z)/\partial z = \{|W_{up}| - |W_{down}|\}/\delta z$ = Wind shear difference across a vertical layer

$\partial M(z)/\partial z = \{M_{up} - M_{down}\}/\delta z$ =

" = Mean molecular weight difference in a vertical layer

δz = Vertical thickness of the atmospheric layers (= 0.25 km assumed)

Dimensionless Numbers of the Flow and Source Characteristics in a Compressible Fluid:

$Ri(z) \equiv \omega_{BVI}^2/\partial W(z)/\partial z\}^2 = \{(g/\theta(z))\cdot\ \partial\theta(z)/\partial z\}/\{\partial W(z)/\partial z\}^2$

" = Gradient Richardson number for isothermal conditions

$Ri(z) = \omega_{BV}^2/\partial W(z)/\partial z\}^2 = \{(g/\theta(z))\cdot\ \partial\theta(z)/\partial z\}/\{\partial W(z)/\partial z\}^2$

" = Gradient Richardson number for non-isothermal conditions

$Ri_b\ (z) \approx \{(g/\theta(z)\}\cdot(\Delta\theta/\Delta z)\}/\{W(z)/\delta z\}^2$

" $\approx \{(g/\theta(z)\}\cdot(\Delta\theta/\Delta z)\}/\{W(z)/\delta z\}^2$

$\therefore$ Ri_b = Bulk Gradient Richardson number with a continuous Brunt-Vaisalla frequency

For vertically isothermal conditions:

$\partial\theta/\partial z = \Gamma_{dry} \equiv g/c_p$ = Dry adiabatic lapse rate since $\Gamma = -\partial T/\partial z = 0$

θ = Potential temperature of "dry" air
c_p = Specific heat of air at constant pressure

$\therefore$ $Ri_b(z) \approx \{(g/\theta)\cdot(g/c_p)\}\{(\delta z/W(z))^2\}$; $\theta \approx T = 250$ K was assumed

For vertically nonisothermal conditions:

$\partial\theta(z)/\partial z = \Gamma_{dry} - \Gamma(z)$; $\Gamma(z) = -\partial T/\partial z$

$\therefore$ $Ri_b(z) \approx \{(g/\theta)(\Gamma_{dry} - \Gamma(z))\}\cdot\{\delta z/W(z)\}^2$

The corresponding critical flow values:

i) Ri_c = 1.0 (Miles, 1986)
" = Critical Richardson number

Previously the accepted critical value of this transitional Richardson number for Kelvin-Helmholtz instability determined to be ¼ as was used by numerous authors (for the transition from laminar to turbulent flow). A necessary, but not a sufficient condition exists for the onset of dynamic instability if the gradient bulk Richardson number is < Ri_c, (Miles, 1986).

ii) Ri_c = 0.50 (Dobbins, 1979)
" = Critical flow Richardson number-For significant amplification of preexisting turbulence levels.

Here we have evaluated the denominator of the gradient Richardson number in a bulk sense for comparison against a critical transitional flow value in order to evaluate the amplification possibilities of preexisting turbulence due to the presence of vertical shear of the horizontal wind. Thus, we have used Ri_c = ½ as the critical Richardson number value (Dobbins, 1979). The denominator of Ri_b has been evaluated using a finite difference approach and the entire expression still retains the thermal stratification information inherent in the Brunt-Vaisalla frequency. This approach will obviously fail to be an acceptable criterion as δz becomes too small since with all else the same, this expression will tend to zero as δz^2 shrinks in the limit to zero thickness. Nevertheless, this criterion can be used in a relative sense to determine flow regions aloft that are dynamically unstable which is exactly what it was proposed to do originally by L.F. Richardson. As written the Bulk gradient Richardson number expression compares the speed of internal gravity waves to that of the mean wind over a layer of specified vertical thickness. Roughly speaking, for known values of the various parameters, this corresponds for a 250 m thick vertical layer to a horizontal wind speed > 10 m/s resulting in dynamical instability (ignoring thermal stratification effects in detail). As can be readily seen in Figures 2 and 8 for summer and winter respectively, this encompasses most of the atmospheric regions aloft with the further restriction in summer of zones of stability located in between layers of dynamical instability.

The precision with which this criterion can be utilized to define the wind shear regions aloft that are dynamically unstable for the generation of the requisite turbulence necessary to radiate acoustic and internal gravity waves is certainly acceptable for a vertical layer

thickness = 0.25 km (see below). Obviously the final result is not independent of the layer thickness chosen, but this is a well known problem that has been evident in Meteorology and Atmospheric Physics for a long time.

Still smaller scale vertical features can certainly be routinely measured, but these features are very hard to input into a global scale model to adequately represent the mean flow conditions for a representative band of latitudes for the tropospheric Polar jet. Finally, this criterion is also only a necessary and not a sufficient condition for the prediction for significant amplification within a region of preexisting turbulence.

Similarly the Rossby no. can be written in terms of the gradient bulk Richardson number in the form:

$Ro = (1/\pi)\cdot\{2.50/(1+Ri_b)\}^{1/2}$ (Stone, 1972)

The source strength parameter, u_o' can be defined using previous related wind shear instability studies in a form that is related to the prevailing wind speed aloft at any level:

$u_o' = 0.01\cdot|W(z)| =$
" = perturbation source horizontal wind as a function of height

This expression is used whenever the region aloft is computed to be dynamically unstable (McIntosh and ReVelle, 1984), otherwise it is set = 0 at all other heights (if dynamic stability aloft exists).

The source description in terms of the gradient bulk Richardson number, the Rossby number and of the perturbation wind radiated at the source are given in Figure 4 for summer and Figure 10 for winter respectively, both plots having been evaluated for non-isothermal atmospheric conditions. Note that in summer-time a zone of stability exists at two very distinct levels aloft where the flow is expected to be fully geostrophic (small Rossby number approximation) whereas in wintertime, the flow is always unstable at all heights for the source properties utilized. Similarly the Rossby number is always < 0.5 at all heights indicating a regime of quasi-geostrophic and hydrostatic flow aloft. Source strength values (written in terms of the perturbation winds) are a direct function of the strength of the winds at all heights, so that they are generally much stronger in winter than in the summer.

Acoustic-Gravity Wave Dispersion Relationship:

The applicable linearized AGW dispersion relationship valid for both the high frequency (acoustic) and low frequency (internal gravity wave) limit with $k_y = 0$ assumed so that λ_y = infinity in the two-dimensional wave modeling, small perturbation amplitude limit is given by (Tolstoy and Herron, 1969; Mihalas and Mihalas, 1984):

$k_z^2(z) = (\omega_{BV}(z)/|W(z)|)^2 - k_x^2 + (\omega(z)^2 - \omega_{AC}(z)^2/c_s(z)^2) =$
" = Square of the vertical wavenumber of the flow = $2\pi/\lambda_z$
λ_z = Vertical wavelength of the system
k_x = Horizontal wavenumber of the flow = $\omega/|W(z)| = 2\pi/\lambda_x$
ω = Angular oscillation wave frequency = $2\pi\cdot f$ (radians/s)
f = Linear oscillation wave frequency (Hz)

***$\lambda_x = 2\pi\cdot|W|/\omega$ = Horizontal wavelength of the wave system**

Propagating Wave Solutions

$s = \int k_z(z)dz$ = Wave system phase factor: Integration from source to observation altitude

***$u'(z) = u_o'(z)\{(k_{zo}\cdot\rho(z))/(k_z(z)\cdot\rho_o)\}^{1/2}\cdot|\cos(s)|$**

" = perturbation wind due to the wave as a function of height

In general in the AGW regime (Mihalas and Mihalas, 1984):

$u'(z) = |\Delta p/p_o|\cdot c_s^{2}\cdot k_x/\{\gamma\cdot\omega\}$

ρ_o = Surface value of the air density (Ground-level)

$p'(z) = u'(z)\{\rho\cdot|W(z)|\}$

" = Perturbation pressure of the wave as a function of height

" = $u_o'(z)\cdot|W(z)\cdot\{\rho_o\cdot\rho(z)\}|^{1/2}\cdot\{k_{zo}/k_z(z)\}^{1/2}\cdot|\cos(s)|$

$P(z) = u_o'(z)\cdot|W(z)\cdot\{\rho_o\cdot\rho(z)\}|^{1/2}\cdot\{k_{zo}/k_z(z)\}^{1/2}\cdot|\cos(s)|$

" = Wave power as a function of height

$I(z) = \{p'(z)\}^2/\{\rho(z)\cdot V_{phx}\}$

" = Wave intensity as a function of height

Evanescent Wave Solutions (Decaying exponentially away from a boundary)

These have not been included in the calculations since these waves are reflected above the ground, but have been listed for completeness.

$s = \int |k_z(z)|dz$ = Wave system phase factor: Integration from source to observation altitude

$u'(z) = u_o'(z)\{(k_{zo}\cdot\rho(z))/(k_z(z)\cdot\rho_o)\}^{1/2}\cdot\exp(-s)$

" = perturbation wind due to the wave as a function of height

$p'(z) = u'(z)\{\rho\cdot|W(z)|\}$

" = Perturbation pressure of the wave as a function of height

" = $u_o'(z)\cdot|W(z)\cdot\{\rho_o\cdot\rho(z)\}|^{1/2}\cdot\{k_{zo}/k_z(z)\}\cdot\exp(-s)|$

$P(z) = u_o'(z)\cdot|W(z)\cdot\{\rho_o\cdot\rho(z)\}|^{1/2}\cdot\{k_{zo}/k_z(z)\}^{1/2}\cdot\exp(-2s)$

" = Wave power as a function of height

$I(z) = \{p'(z)\}^2/\{\rho(z)\cdot V_{phx}\}$

" = Wave intensity as a function of height

In this preliminary study, we have not interpreted our results for either the power or intensity values that were predicted from the expressions given above. These values had already been evaluated by Tolstoy and Herron (1969) and were shown to be compatible with the jet stream as an unstable dynamic wind shear source for producing internal gravity wave pressure waves at the ground. We have also not interpreted the evanescent wave contributions since these waves do not arrive at ground-level, but are refracted upward back toward the source.

Finally, we can physically interpret the expression for the source perturbation wind, Uo'(z), in terms of wave kinetic energy density conservation (=$1/2\cdot\rho\cdot\{u_o'\}^2$) during propagation in a horizontally stratified, steady state, atmosphere. If the vertical wavenumber (= $2\pi/\{m\cdot\lambda_z\}$) is an integral multiple of the source height distance above the ground, r, for m = 1, 2, 3, … then we can write the above expression in the form:

$$u'(z) = u_o' \cdot \{(\rho_o \cdot r_o)/(\rho(z) \cdot r)\}^{1/2}$$

This latter expression is exactly what would be expected for an inviscid, non-heat conducting fluid for a linear wave propagating from an infinite length line source, i.e., in cylindrical coordinates the decay of the wave perturbation wind (or of the pressure wave amplitude) must possess an $r^{-1/2}$ dependence , where r_o is a reference distance scale (close to the source region) and r is the total distance from the source to the observer.

III. Results of Calculations

These equations have been solved in a FORTRAN computer code: GPRSWND3.f and solved for the following explicit cases:

Mean summertime and winter-time conditions in middle latitudes (in all cases including mean zonal winds only since generally the East-West component zonal winds are much stronger than the corresponding North-South meridional component winds):

a) Isothermal atmosphere with isothermal AGW resonant frequencies
b) Nonisothermal atmosphere and nonisothermal AGW resonant frequencies

We have also computed the results for a nonisothermal atmosphere while using the isothermal resonant frequencies for AGW's. These results that have not been formally included in this report most closely resemble those of case a) above at least in terms of the predicted ground-level pressure wave amplitudes.

The coordinate axes in each case are the assumed geopotential source heights on the ordinate as a function of the predicted ground-level pressure wave amplitudes in Pa on the abscissa in the upper panel (Figures 5-6 for summer and Figures 11-12 in winter) and the corresponding ground-level pressure wave periods in minutes in the lower panel. Figures 5 and 11 correspond to case a) above and Figures 6 and 12 correspond to case b) above respectively.

Conclusions: All the graphs within each group have similar shapes but with different predicted ground-level pressure wave amplitudes due to the different equation set and the corresponding atmospheric properties utilized. The equation set solved explicitly for the non-isothermal atmosphere utilizing the non-isothermal atmospheric resonant frequencies described in terms of linear vertical temperature gradients within each layer is likely to be the most reliable set of predictions that we can make given the comparatively simple analytic source model.

We have not yet been able to determine explicitly why there is so much difference in the amplitude of the predicted ground-level pressure waves in summer whereas in winter there is very little difference between the methods, although the4r are slight decreases in the predicted amplitude in winter for case b). The summertime difference is apparently due to the atmospheric structure differences between the two seasons however since the shapes of the ground-level pressure wave predictions are so similar in Figures 5 and 6.

Summertime Results:

The largest wave amplitudes predicted at the ground are ~0.30 Pa (case a) and 0.08 Pa (case b). Each of these pressure wave maxima extend over a broad range of periods from ~5 to 30 minutes and emanate from a source altitude of 10-12 km (from the Tropospheric jet stream source due to mechanically generated wind shear dynamic instability). Wavelengths from 7.5 to 25 km were computed at corresponding wave periods from ~5 to > 100 minutes over the entire source height range from the ground to 100 km.

Winter-time Results:

The largest wave amplitudes predicted at the ground are ~3-8 Pa (case a) and 2-7 Pa (case b). Each of these pressure wave maxima extend over a broad range of periods from ~5 to 30 minutes and emanate from a source altitude of 8-10 km (from the Tropospheric jet stream source due to mechanically generated wind shear dynamic instability) as well as from 40-60 km, but then ONLY at periods of about 5-7 minutes for all of these later cases and consequently not a broadband source. Wavelengths from 5 to 25 km were computed at corresponding wave periods from ~5 to > 100 minutes over the entire height range from the ground to 100 km.

Thus, we have definitely identified a broad-band pressure wave source, the Tropospheric Polar jet stream which can generate the requisite waves by indirect forcing (IF) in the atmospheric through the mechanism of internal gravity waves generated by dynamic shear instability aloft. There should be some hemispheric differences in the oceanic surface wave heights that are generated by this mechanism because the amplitudes in summer are consistently smaller, but they still extend over a large range of wave periods. We can imagine that the southern hemisphere should develop stronger wave heights by direct forcing because of the large fetch of open waters due to the lack of continents, but this probably also applies to IF too. Thus, for the Southern hemisphere perhaps smaller pressure wave amplitudes are sufficient since there are fewer massive obstacles to stop the oceanic waves once they get generated unlike the Northern hemisphere with its large land masses.

We have not yet included the nocturnal low-level jet stream winds that are found at heights from ~ 200 m to 1.5 km aloft (Gill, 1982) in any of these pressure wave calculations since its corresponding horizontal length scale is not global and because it is generally only active for a much shorter time period, whereas the Polar Tropospheric jet stream is truly a global (synoptic) scale phenomenon that is always present. These latter winds are directed from West to East in both hemispheres simultaneously although the speed is ~2 times slower in the summer season and concentrated at a slightly different altitude.

IV. Summary and Conclusions

We have computed the expected pressure wave amplitude and the associated wave periods for the atmospheric forcing of the oceans by means of an indirect forcing by an internal gravity wave mechanism using an analytical model originally developed by Herron and Tolstoy (1969). This technique was adapted for our purposes using non-isothermal AGW resonant periods in a non-isothermal atmosphere (Mihalas

and Mihalas, 1984). These calculations were done in order to determine if such waves could excite infragravity waves in the ocean which have previously been determined to excite continuous oscillations of the solid earth (Tanimoto and ReVelle, 2004).

V. References:

Dobbins, R.A., Atmospheric Motion and Air Pollution, John Wiley and Sons, New York, 323 pp., 1979.

Gavrilov, N.M., Parameterization of momentum and energy depositions from gravity waves generated by tropospheric hydrodynamic sources, Ann. Geophysicae, 15, 1570-1580, 1997.

Gill, A.E., Atmosphere-Ocean Dynamics, Academic Press, Inc., Orlando, FL, 662 pp., 1982.

Grigor'ev, G.I., Acoustic-Gravity Waves in the Earth's Atmosphere (Review), Radiophys. and Quantum Electron., 42, 1-21, 1999.

Herron, T.J. and I. Tolstoy, Tracking Jet Stream Winds from Ground Level Pressure Signals, J. Atmos. Sci., 26, 266-269, 1969.

Herron, T.J., I. Tolstoy and D.W. Kraft, Atmospheric Pressure Background Fluctuations in the Mesoscale Range, J. Geophys. Res., 74, 1321-1329, 1969.

Hines, C.O., Nonlinearities and Linearities in Internal Gravity Waves of the Atmosphere and Oceans, Geophys. and Astrophys. Fluid Dynamics, 96, 1-30, 2002.

Lindzen, R.S., Multiple gravity-wave breaking levels, J. Atmos. Sci., 42, 301-305, 1985.

McIntosh, B.A. and D.O. ReVelle, Traveling Atmospheric-Pressure Waves Measured During a Solar Eclipse, J. Geophys. Res., 89, 4953-4962, 1984.

Mihalas, D. and B. Weibel-Mihalas, Foundations of Radiation Hydrodynamics, Dover Publications, Inc., Mineola, New York, 718 pp., 1984.

Miles, J., Richardson Criterion for the Stability of Stratified Shear-Flow, 29, 3470-3471, 1986.

Musielak, Z.E., R. Rosner, R.F. Stein and P. Ulmschneider, On Sound Generation by Turbulent Convection: A New Look at Old Results, Astrophysical Journal, 423, 474-487, 1994.

Nappo. C.J., An Introduction to Atmospheric Gravity Waves, Academic Press, Amsterdam, 276 pp., 2002.

Petterssen, S., Introduction to Meteorology (Third Edition), McGraw-Hill Book Co., New York, 333 pp., 1969.

Stein, R.F., Generation of Acoustic and Gravity Waves by Turbulence in an Isothermal Stratified Atmosphere, Solar Physics, 2, 385-432, 1967.

Stone, P.H., A Simplified Radiative-Dynamical Model for the Static Stability of Rotating Atmospheres, J. Atmos. Sci., 31, 1681-1690, 1972.

Tanimoto, T. and D.O. ReVelle, The Oceanic Excitation Hypothesis for the Continuous Oscillations of the Earth, Submitted to Geophys. J. International, 2004.

Tolstoy, I. and T.J. Herron, A Model for Atmospheric Pressure Fluctuations in the Mesoscale Range, J. Atmos. Sci., 26, 270-273, 1969.

Weinstock, J., Spectra and a Global Source of Gravity Waves for the Middle Atmosphere, Adv. Space Res., 17, 1167-1176, 1996.

VI. Acknowledgments

The primary author would like to thank the IGPP program at Los Alamos National Laboratory for providing funds for this project for the past three years. He would also like to thank Professor Tanimoto for his kindness and hospitality during my visits to the University of California at Santa Barbara on two separate occasions during the course of this research.

VII. Appendix A. Atmospheric Properties:

Below are listed the specific FORTRAN subroutines for calculating the mean atmospheric properties in summer and winter for temperature, the vertical temperature gradient and for the zonal wind speed, all as a function of the geopotential height.

```
C*************************************************************************
C     Subroutine WSEASON and SSEASON computes the very high cross-correlation,
C     curve-fit value of the vertical temperature gradient in winter and in
C     summer from the ground up to at least 140 km.
C*************************************************************************
      SUBROUTINE WSEASON( C, B, E, X)
      REAL*8 C, B, E, X
C     C = AT, B = DTDZ, E = WIND(I), X = Z(I)
      COMMON AT,DTDZ,WIND,Z
       C = -3.266696E-16*X**10.0+2.072790E-13*X**9.0-5.567942E-11*
     +    X**8.0+8.271596E-09*X**7.0-7.464375E-07*X**6.0
     +    +4.229622E-05*X**5.0-1.468348E-03*X**4.0+2.558343E-02*
     +    X**3.0+3.689213E-02*X**2.0-6.797700E+00*X+274.8593
       B = -3.266696E-15*X**9.0+1.865511E-12*X**8.0-4.454354E-10*
     +    X**7.0+5.790117E-08*X**6.0-4.4786253E-06*X**5.0+2.114811E-04*
     +    X**4.0-5.873392E-03*X**3.0+7.675029E-02*X**2.0+7.378426E-02*X
     +    -6.797700E+00
       E = -8.466203E-16*X**10.0+5.266636E-13*X**9.0-1.380927E-10*
     +     X**8.0+1.991154E-08*X**7.0-1.735234E-06*X**6.0+9.539013E-05*X
     +     **5.0-3.386100E-03*X**4.0+7.770110E-02*X**3.0-1.064479E+00*X
     +     **2.0+7.471115E+00*X+5.571346E-01
        RETURN
       END
C*************************************************************************
      SUBROUTINE SSEASON( C, B, E, X)
      REAL *8 C, B, E, X
C     C = AT, B = DTDZ, E = WIND, X = Z(I)
      COMMON AT,DTDZ,WIND,Z
      C = -5.875750E-17*X**10.0+3.442560E-14*X**9.0-8.009312E-12*
     +    X**8.0+9.251030E-10*X**7.0-5.455385E-08*X**6.0
     +    +1.572698E-06*X**5.0+2.868723E-06*X**4.0-5.820824E-03*
     +    X**3.0+4.248800E-01*X**2.0-9.563706E+00*X+300.6343
       B = -5.875750E-16*X**9.0+3.098304E-13*X**8.0-6.407450E-11*
     +    X**7.0+6.475721E-09*X**6.0-3.273231E-07*X**5.0
     +    +7.863490E-06*X**4.0+1.147489E-05*X**3.0-1.746247E-02*
     +    X**2.0+8.497600E-01*X-9.563706E+00
       E = 7.315382E-11*X**6.0+1.192039E-08*X**5.0
     +    -1.411983E-05*X**4.0+2.564756E-03*X**3.0-1.591690E-01*
     +    X**2.0+2.644623E+00*X+2.926475
        RETURN
       END
C     ***************************************************************
C     MOLECULAR WEIGHT SUBROUTINE: SEASON INDEPENDENT computes the very high
```

```
C     cross-correlation, curve-fit value of the mean molecular weight up to at
C     least 140 km, independently of the season (actually it is dependent on
the
C     time of the day since it is so dependent on the diurnal solar cycle.
       SUBROUTINE MWEIGHT (B, Y)
       REAL*8 B, Y
C      B = MW, Y = Z(I)
       COMMON MW,Z
       B = -6.459684E-18*Y**10.0+3.603999E-15*Y**9.0-8.310390E-13*Y**8.0
      +    +1.026909E-10*Y**7.0-7.378242E-09*Y**6.0+3.123649E-07*Y**5.0
      +    -7.496962E-06*Y**4.0+9.097271E-05*Y**3.0-3.965730E-04*Y**2.0
      +    -4.378229E-04*Y+28.96842
       RETURN
       END
C     ***********************************************************************
```

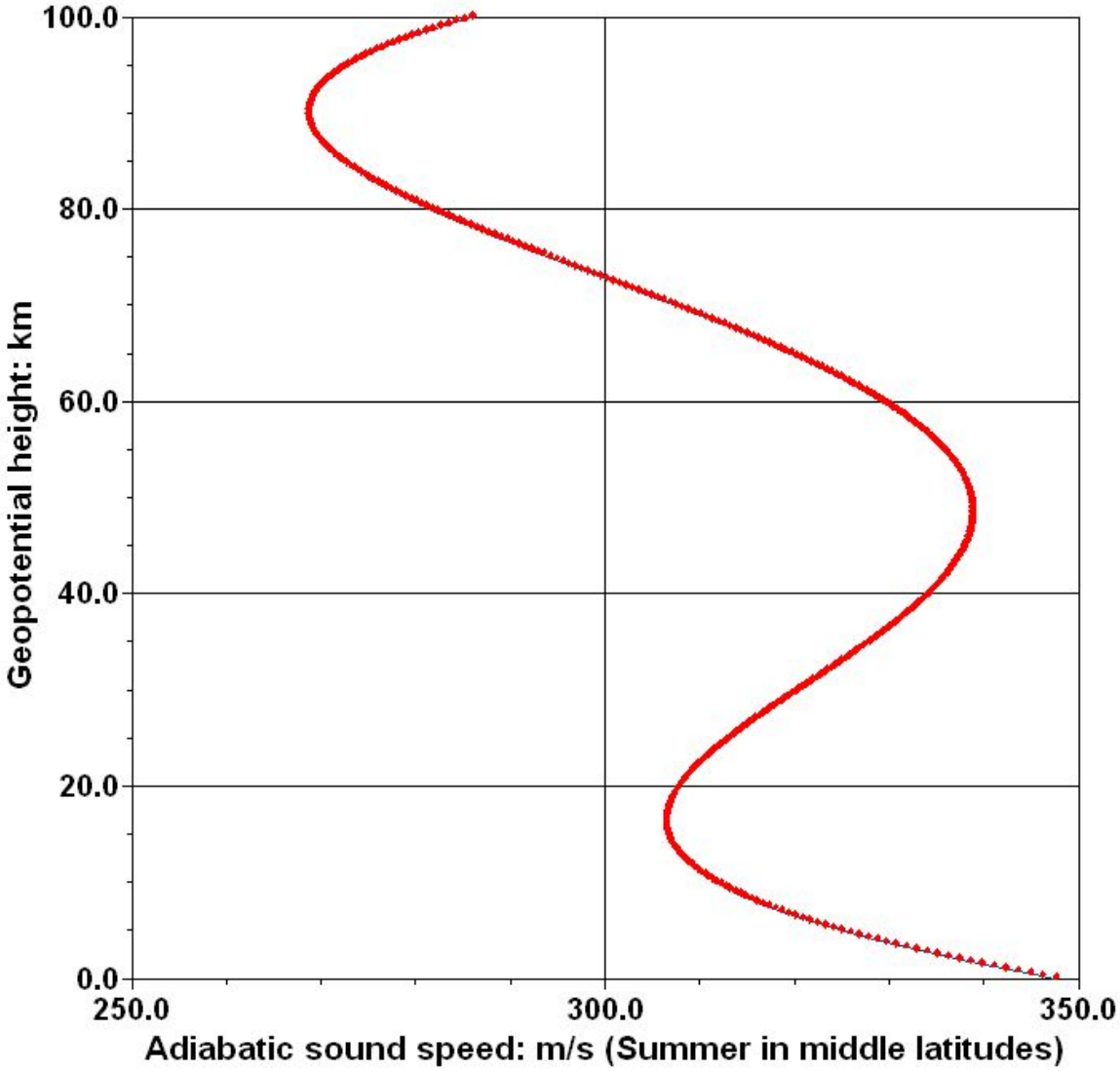

Figure 1: Adiabatic sound speed as a function of height in summer.

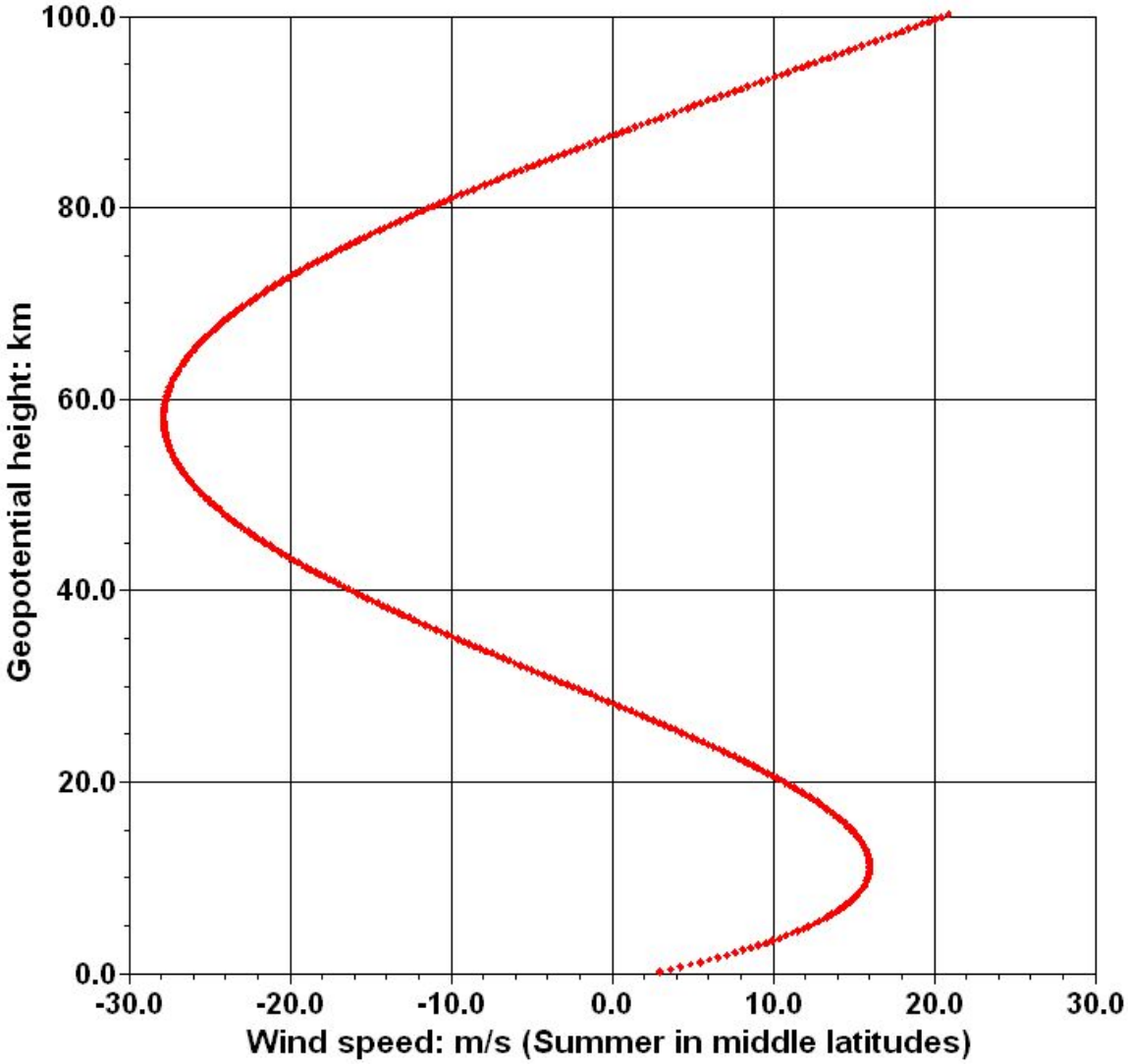

Figure 2: Horizontal wind speed as a function of height in summer.

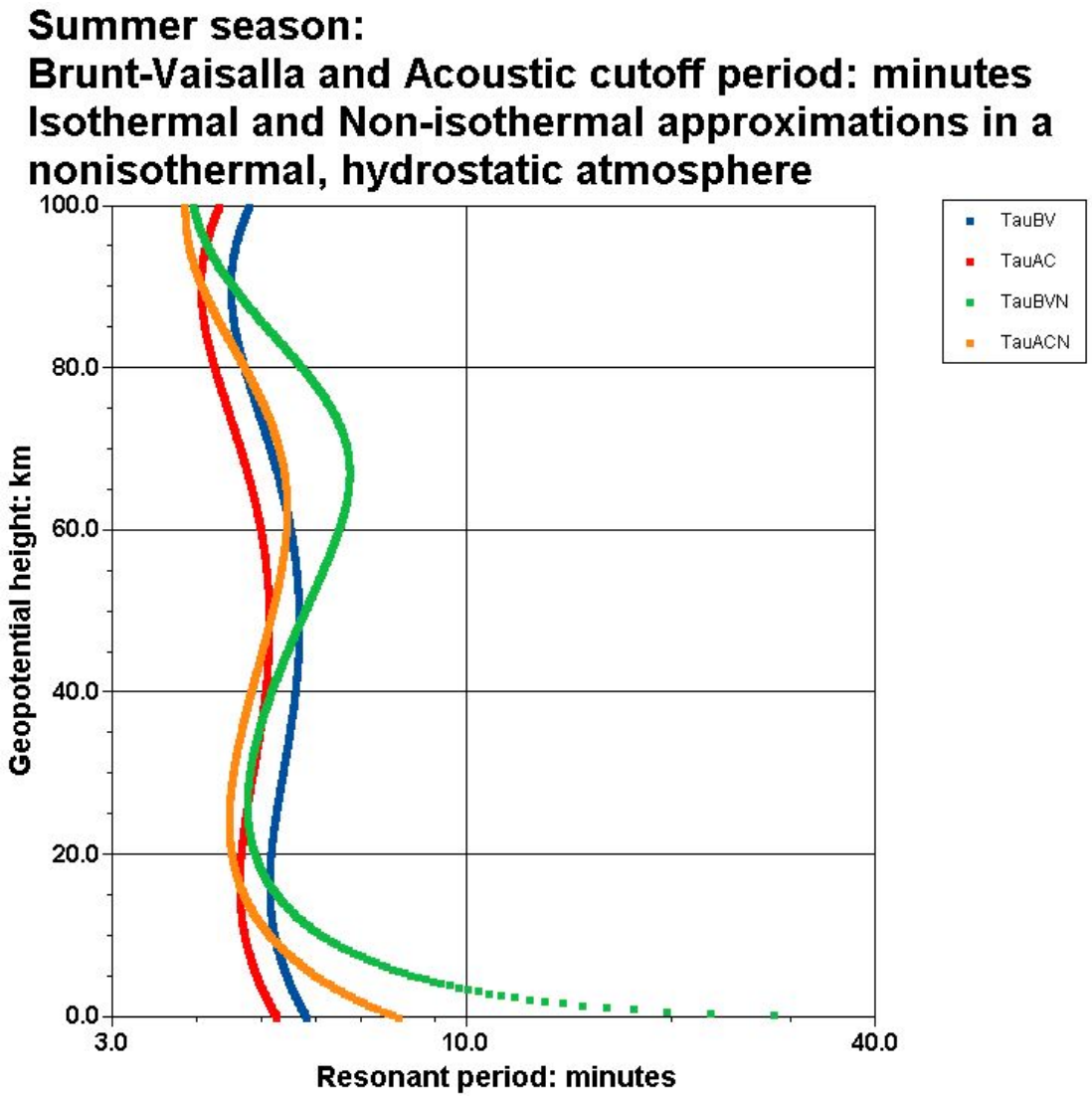

Figure 3: Atmospheric resonant frequencies as a function of altitude in summer.

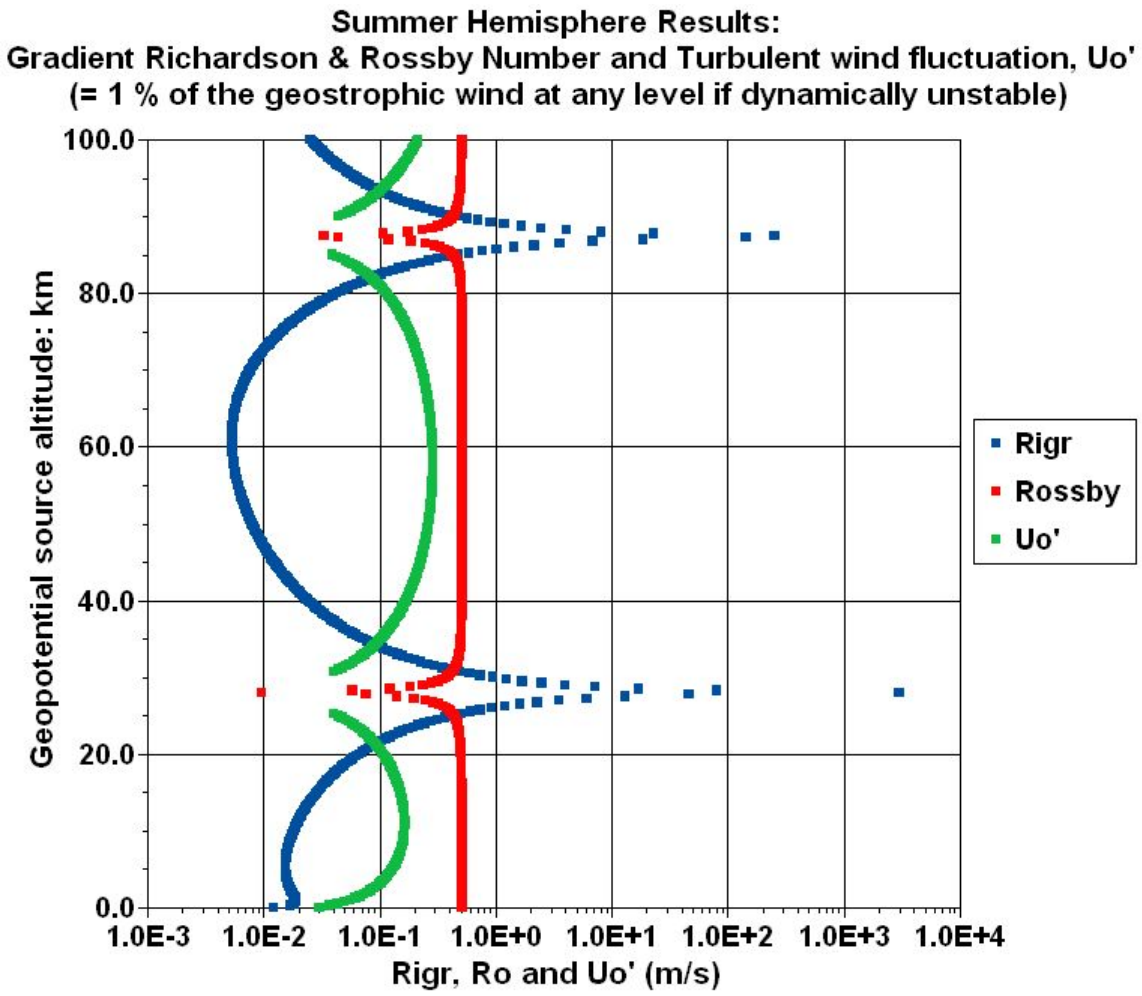

Figure 4: Gradient bulk Richardson number, Rossby number and the corresponding perturbation wind source due to dynamic shear instability aloft in summer for non-isothermal atmospheric conditions.

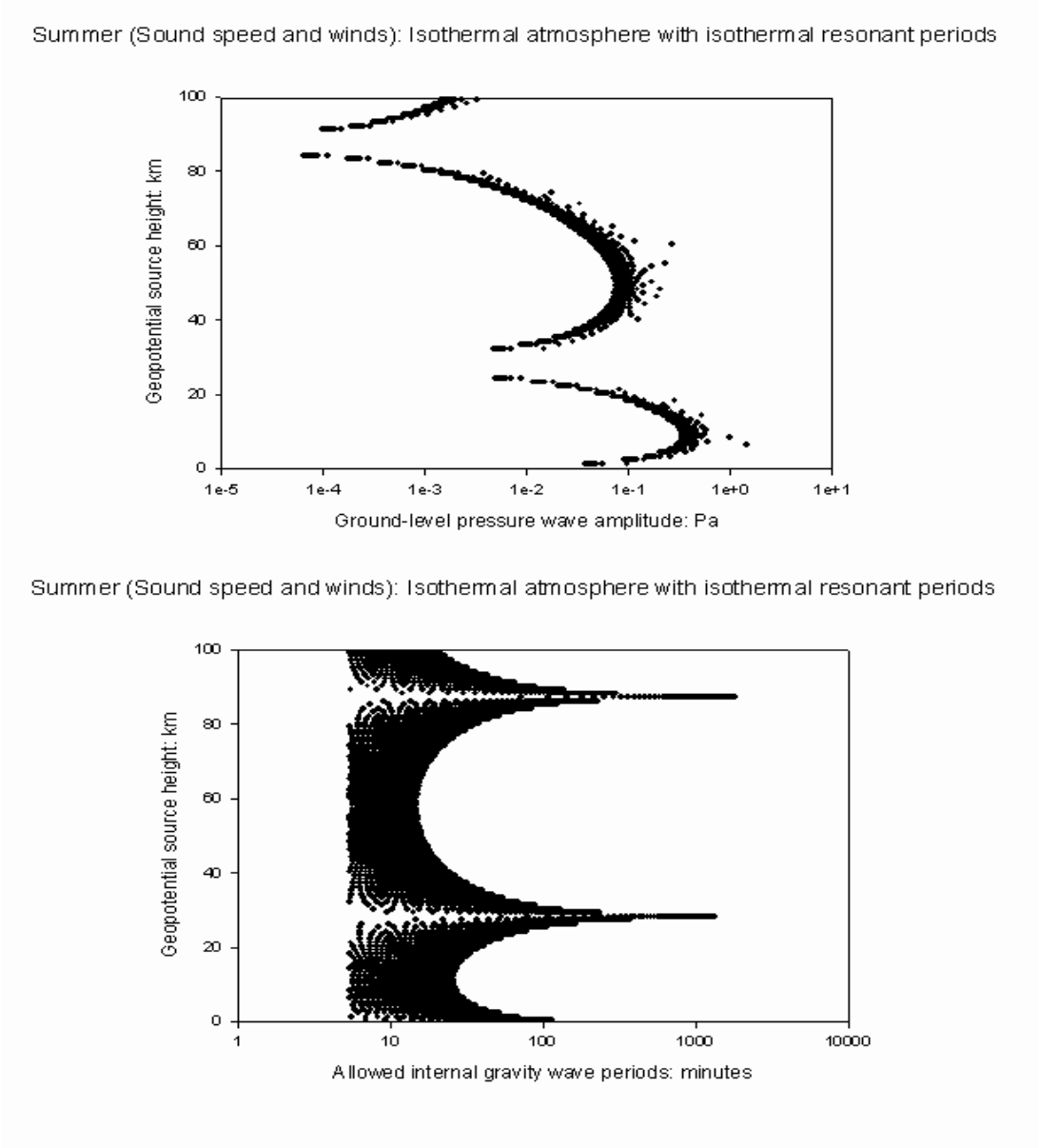

Figure 5: Isothermal atmosphere model with an isothermal resonant frequency approximation assumed in the AGW dispersion relationship: Upper panel: Predicted ground-level pressure wave amplitude as a function of the source height in summer; Lower panel: Corresponding wave period in minutes as a function of the source height in summer.

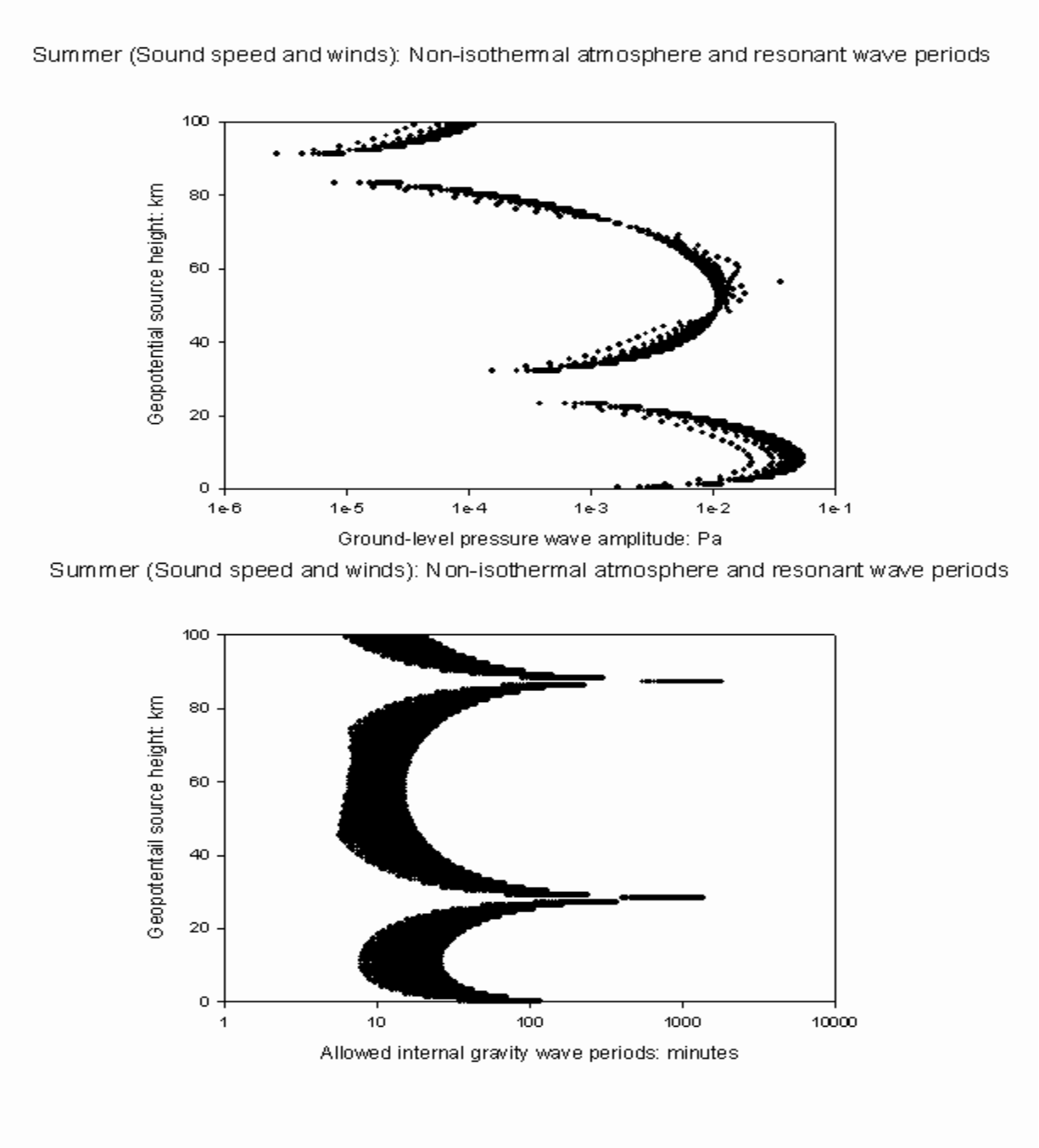

Figure 6: Non-isothermal atmosphere model with the non-isothermal resonant frequency approximation assumed in the AGW dispersion relationship: Upper panel: Predicted ground-level pressure wave amplitude as a function of the source height in summer; Lower panel: Corresponding wave period in minutes as a function of the source height in summer.

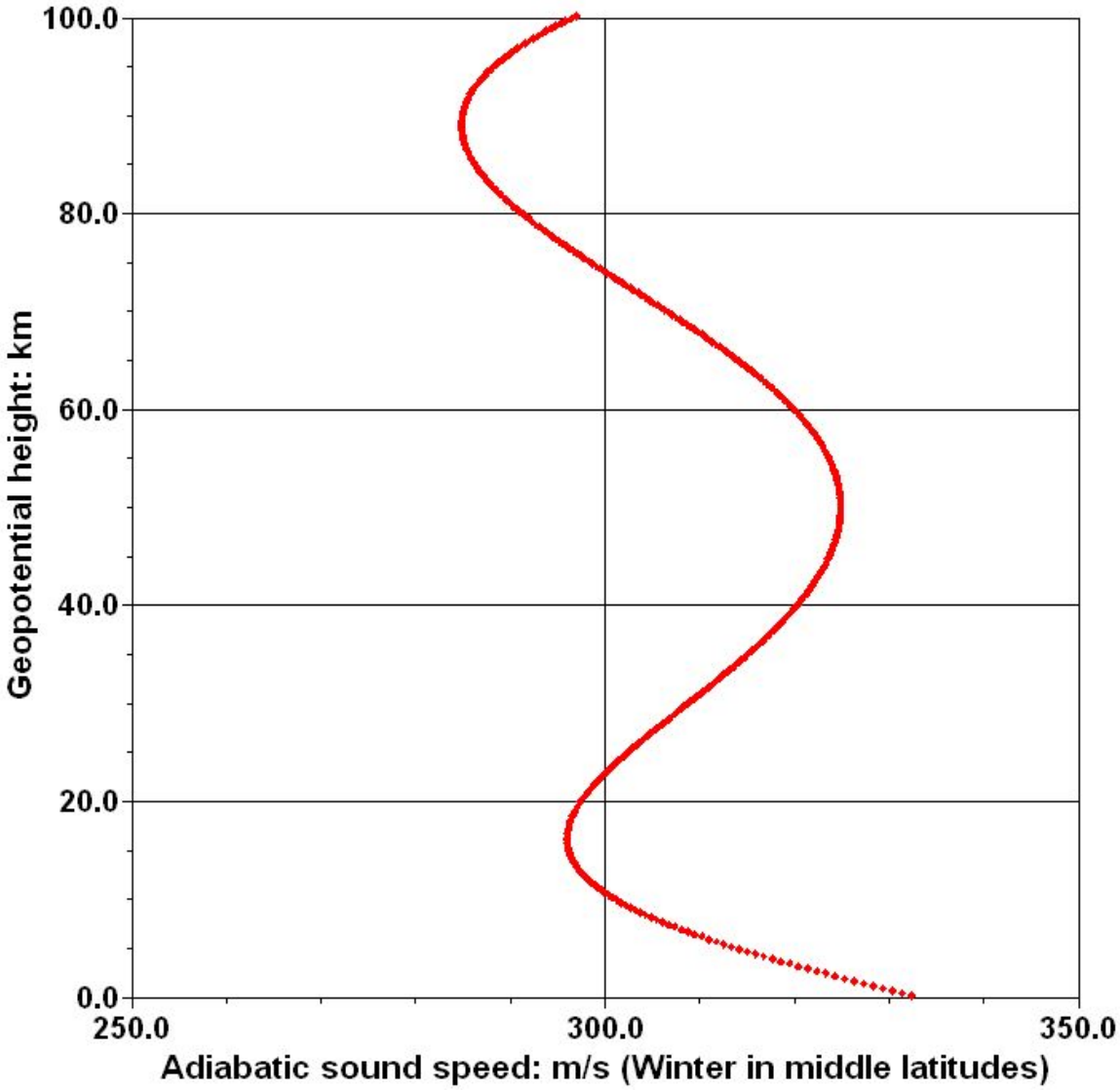

Figure 7: Adiabatic sound speed as a function of height in winter.

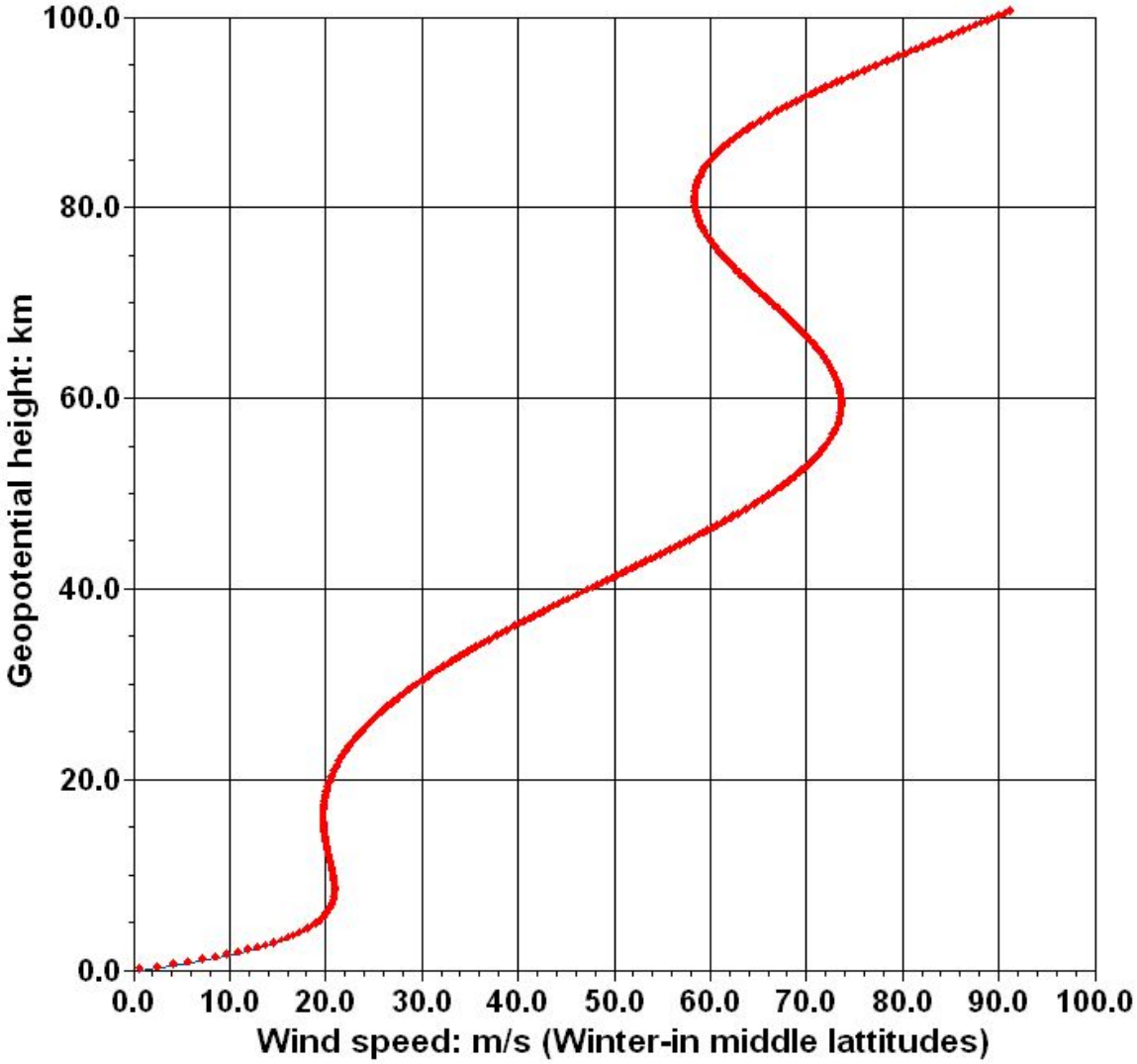

Figure 8: Horizontal wind speed as a function of height in winter.

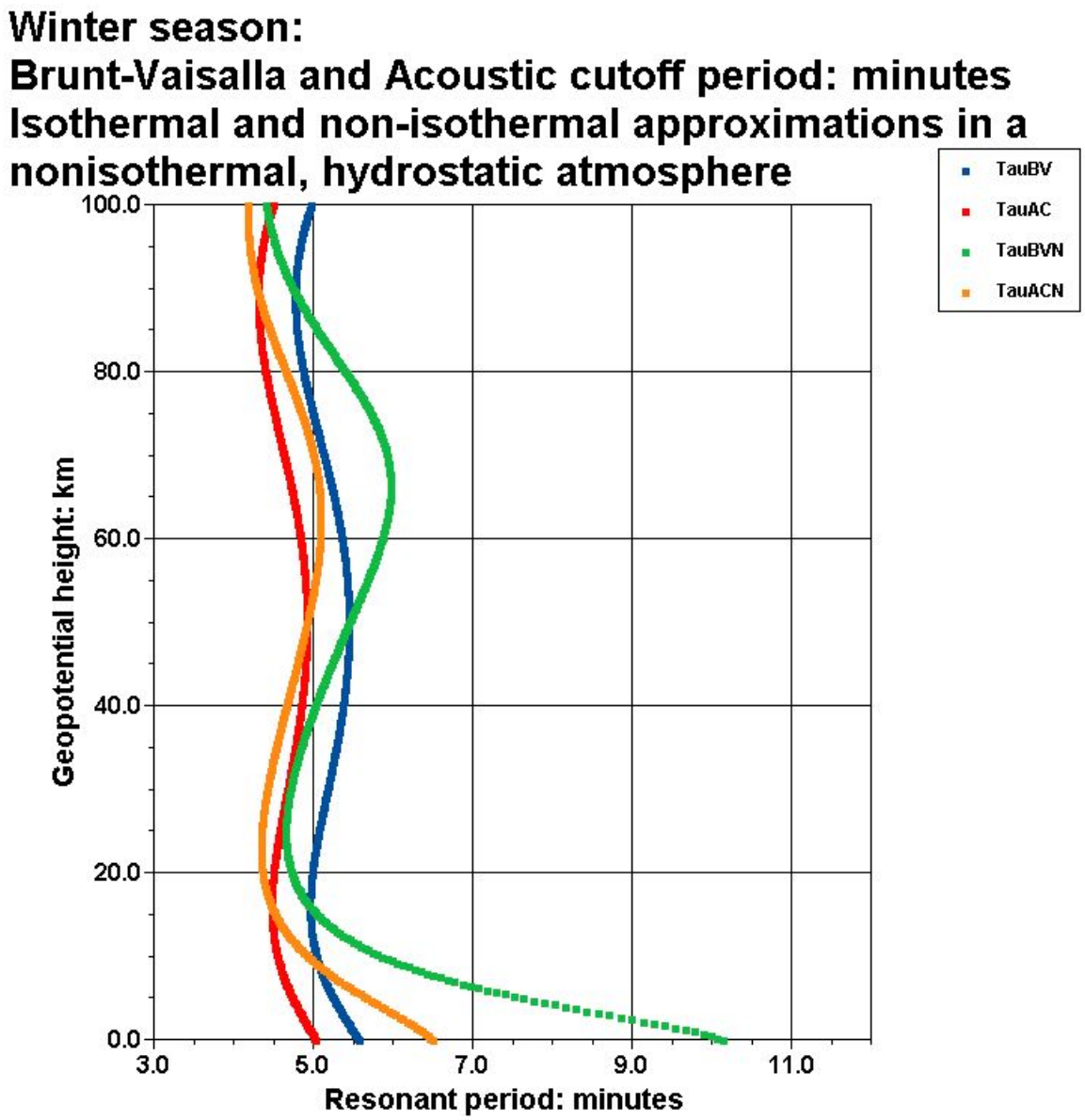

Figure 9: Atmospheric resonant frequencies as a function of altitude in winter.

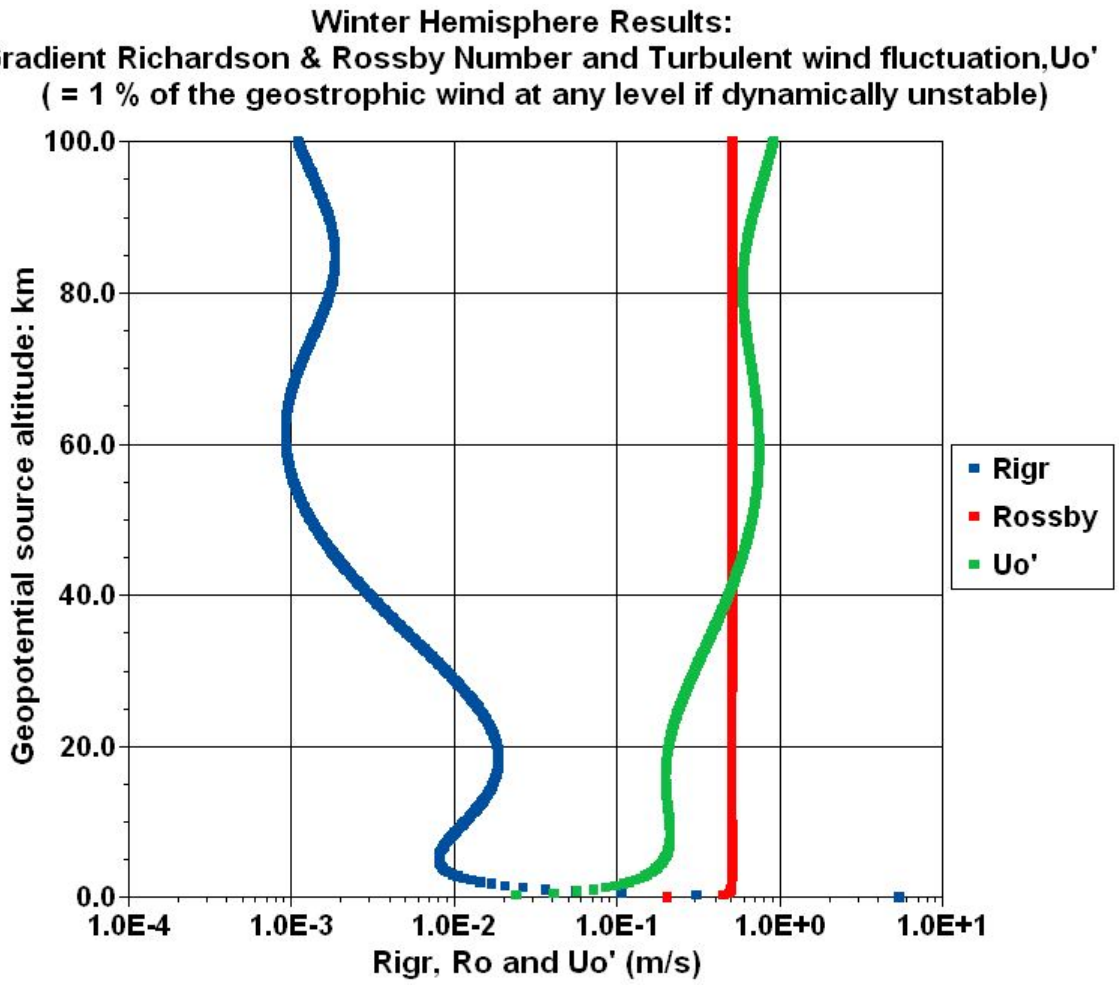

Figure 10: Gradient bulk Richardson number, Rossby number and the corresponding perturbation wind source due to dynamic shear instability aloft in winter for nonisothermal conditions.

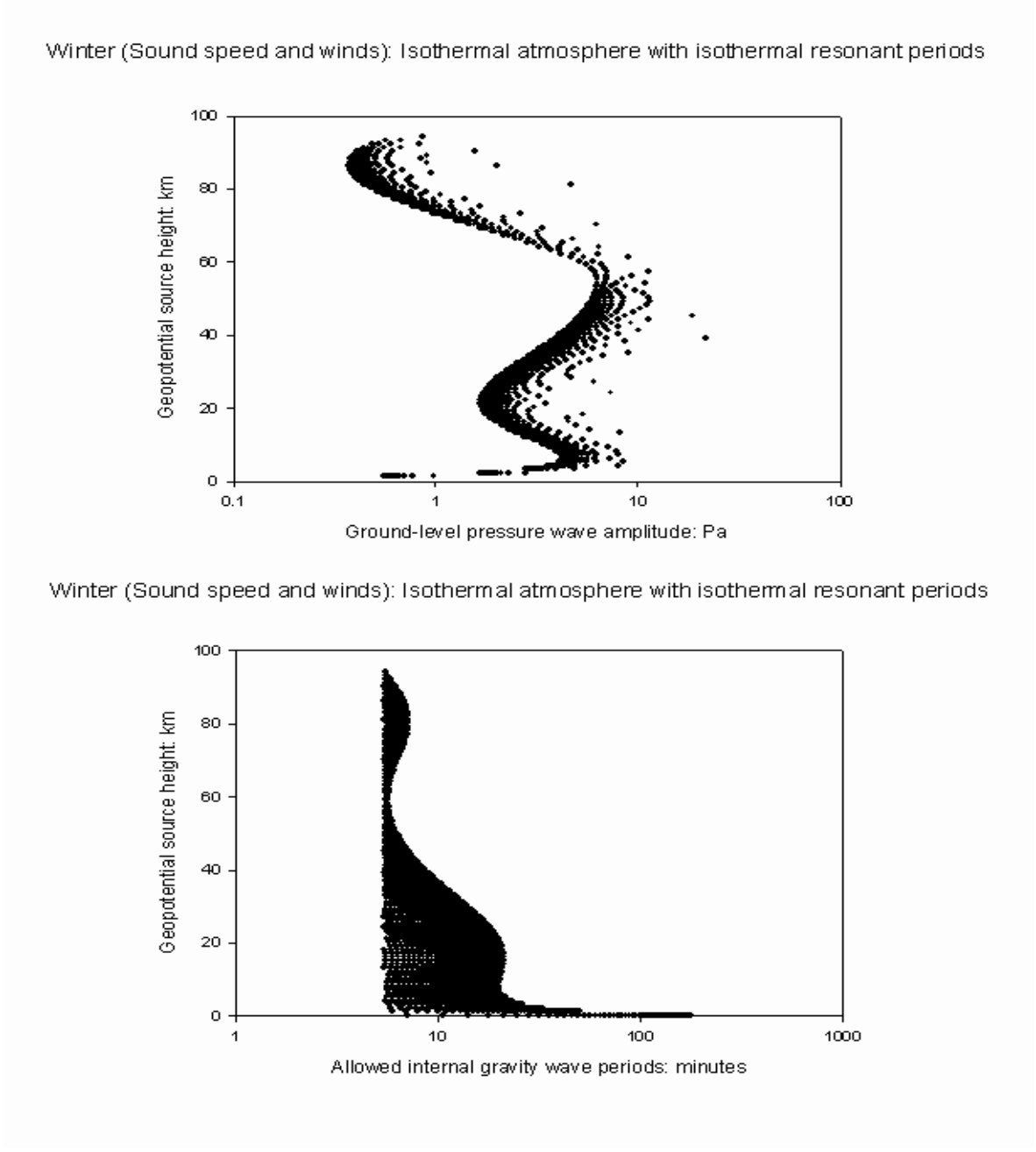

Figure 11: Isothermal atmosphere model with an isothermal resonant frequency approximation assumed in the AGW dispersion relationship: Upper panel: Predicted ground-level pressure wave amplitude as a function of the source height in summer; Lower panel: Corresponding wave period in minutes as a function of the source height in winter.

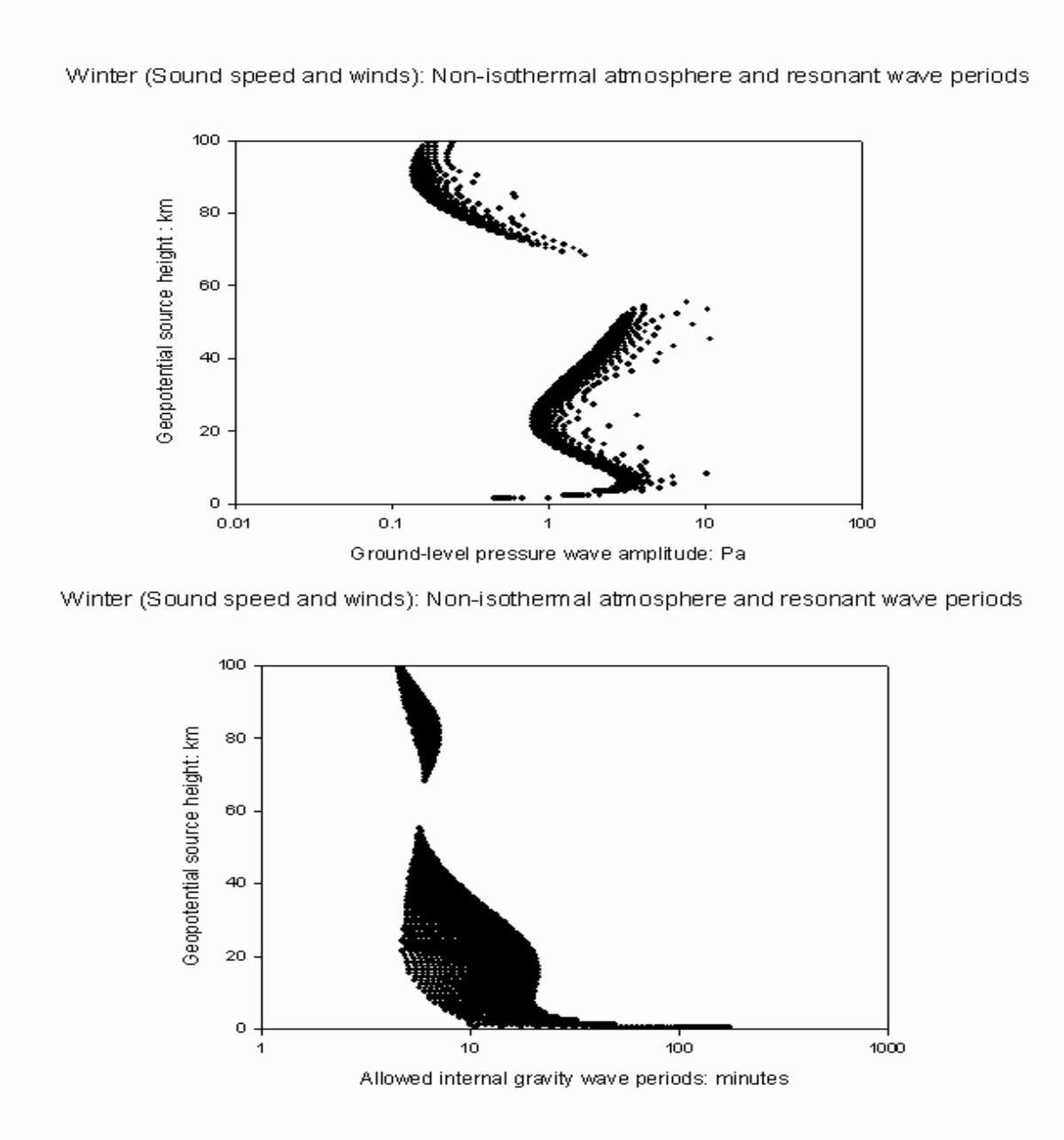

Figure 12: Non-isothermal atmosphere model with the non-isothermal resonant frequency approximation assumed in the AGW dispersion relationship: Upper panel: Predicted ground-level pressure wave amplitude as a function of the source height in summer; Lower panel: Corresponding wave period in minutes as a function of the source height in winter.